



1 **Determining the threshold of issuing flash flood**
2 **warnings based on people's response process**
3 **simulation**

4
5 Ruikang Zhang^{a, b}, Dedi Liu^{a, b, c*}, Lihua Xiong^{a, b}, Jie Chen^{a, b}, Hua Chen^{a, b}, Jiabo
6 Yin^{a, b}

7
8 ^aState Key Laboratory of Water Resources Engineering and Management, Wuhan University,
9 Wuhan, China

10 ^bHubei Provincial Key Lab of Water System Science for Sponge City Construction, Wuhan
11 University, Wuhan, China

12 ^cDepartment of Earth Science, University of the Western Cape, Robert Sobukwe Road,
13 Bellville 7535, Republic of South Africa

14
15 * Correspondence to Dedi Liu: dediliu@whu.edu.cn

16



17 **Abstract:** The effectiveness of flash flood warnings depends on the people's response
18 processes to the warnings. And false warnings and missed events cause the people's
19 negative responses. It is crucial to find a way to determine the threshold of issuing the
20 warnings that reduces the false warning ratio and the missed event ratio, especially for
21 uncertain flash flood forecasting. However, most studies determine the warning
22 threshold based on the natural processes of flash floods rather than the social
23 processes of warning responses. Therefore, an agent-based model (ABM) was
24 proposed to simulate the people's response processes to the warnings. And a
25 simulation chain of "rainstorm probability forecasting - decision on issuing warnings -
26 warning response processes" was conducted to determine the warning threshold based
27 on the ABM. Liulin Town in China was selected as a case study to demonstrate the
28 proposed method. The results show that the optimal warning threshold decreases as
29 the forecasting accuracy increases. And as the forecasting variance or the variance of
30 the forecasting variance increases, the optimal warning threshold decreases (increases)
31 for low (high) forecasting accuracy. Adjusting the warning threshold according to the
32 people's tolerance levels of the failed warnings can improve warning effectiveness,
33 but the prerequisite is to increase the forecasting accuracy and decrease the
34 forecasting variance. The proposed method provides valuable insights into the
35 determination of warning threshold for improving the effectiveness of flash flood
36 warnings.

37 **Keywords:** Threshold of issuing warnings; Flash flood warnings; People's response
38 processes; Evacuation; Agent-based model



39 1. Introduction

40 With the intensification of climate change and human activities (Slater et al.,
41 2021), flash floods have become one of the most serious disasters threatening
42 economic and social security (Borga et al., 2019). Flash flood warning has been taken
43 as an effective and economical means of preventing flash flood disasters (Yin et al.,
44 2023). By issuing warnings before the occurrence of flash floods, people are advised
45 to or ordered to evacuate for reducing the casualties. However, the people's responses
46 to the warnings are complex processes including receiving the warnings,
47 understanding the warnings, trusting the warnings, and personalizing the flood risk
48 (Mileti, 1995; Parker et al., 2009). And these complex processes might hinder the
49 evacuation and undermine the effectiveness of the warnings (Cools et al., 2016). To
50 improve the effectiveness of flash flood warnings, extensive studies have been done
51 to pursue higher accuracy and longer lead time of flash flood forecasting (Han and
52 Coulibaly, 2017; Lei et al., 2018). Unfortunately, the people's responses to the
53 warnings have rarely been explored and have become a bottleneck in improving the
54 effectiveness of the warnings and reducing casualties (Bodoque et al., 2019; Wang et
55 al., 2022).

56 The people's negative responses to the warnings have been mainly attributed to
57 the uncertainties of the flash flood forecasting and the warnings. The uncertainties of
58 flash flood forecasting are from the uncertainties of meteorological forecasting,
59 observation data, initial conditions, hydrological and hydraulic model structure, model
60 parameters, and so on (Boelee et al., 2019). To describe the uncertainties of flood
61 forecasting, a probabilistic flood forecasting was proposed and had been widely
62 applied in the issuing warnings by the disaster prevention administrators
63 (Krzysztofowicz, 2001). If the probability of flash flood disasters from the
64 probabilistic flood forecasting exceeds a preset threshold, the procedure of the issuing
65 warning will be triggered (Coccia and Todini, 2011; Todini, 2017). If the threshold is
66 set low, even a low forecasted probability of flash flood disasters can exceed the
67 threshold, and lots of warnings with only the low probability of flash flood disaster
68 will be issued, resulting in an increase in the false warning ratio. In contrast, if the
69 threshold is set high, only the flash flood disasters with high forecasted probability
70 can be warned, and some flash flood disasters with not low probability will be missed,
71 leading to an increase in the missed event ratio (Potter et al., 2021). These two



72 increases from both the false warning ratio and the missed event ratio can decrease the
73 people's responses to the warnings and expand the casualties. Simmons and Sutter
74 (2009) conducted a statistical analysis of tornado data from 1986 to 2004, and they
75 found that tornadoes with a higher false warning ratio killed and injured more people.
76 LeClerc and Joslyn (2015) explored the cry wolf effect in weather-related decision
77 making through a controlled experimental approach. And their experiments revealed
78 that the decreasing false warning ratio could increase people's trust in the warnings
79 when the trust level was in the medium range, while both too high and too low false
80 warning ratios led to inferior decision making. Ripberger et al. (2015) found that the
81 false warning ratio and the missed event ratio significantly reduced people's trust in
82 the National Weather Service, and suppressed their positive responses via a large
83 regional survey. However, it is impossible to simultaneously reduce the false warning
84 ratio and the missed event ratio at a certain level of forecasting, as there is a trade-off
85 between these two ratios as described above. Therefore, it is crucial to find a way to
86 determine an appropriate threshold that balances the false warning ratio and the
87 missed event ratio for improving the positive warning responses and reducing the
88 disaster casualties.

89 Extensive methods have been proposed to determine the threshold of issuing
90 flood warnings for balancing the false warning ratio and the missed event ratio (Duc
91 Anh et al., 2020; Ke et al., 2020; Ramos Filho et al., 2021; Tekeli and Fouli, 2017;
92 Young et al., 2021). The methods have gradually evolved from fixed threshold
93 determination methods to dynamic threshold determination methods, and from
94 data-driven methods to simulation-based methods (Cheng, 2013). However, these
95 methods only determined the threshold of issuing warnings based on the natural
96 processes of flash floods, while ignoring the social processes of warning responses.
97 The goal of flash flood warnings is to stimulate the people's responses to the warnings
98 for reducing casualties. Even a reliable warning cannot be effective without people's
99 positive responses to it. To our best knowledge, there are very few methods to
100 determine the threshold based on people's response process simulation. Roulston and
101 Smith (2004) generalized the warning release into an improved classical binary
102 cost-loss problem, where the people's warning response level was expressed as a
103 function of false warning ratio, and this warning response level variable was included
104 in the cost-loss analysis. And the threshold of issuing warnings was derived with the
105 goal of minimizing the cost loss ratio under different scenarios. Sawada et al. (2022)



106 proposed a stylized model that coupled natural and social systems to determine the
107 threshold of issuing warnings. In this stylized model, the warning response level was
108 attributed to be influenced by both the success rate of the warning and the flood
109 experience, and then was mapped to flood losses through an empirical equation.
110 However, these studies only described the warning response level through empirical
111 equations or conceptual models, instead of describing the warning response processes
112 through process-based models. To reflect the characteristics of flash flood disaster
113 prevention and the flash flood warning responses, it is necessary to simulate the
114 people's response processes of receiving warnings, making evacuation decisions,
115 implementing evacuation, and being submerged by flash floods (or reaching shelters).

116 Agent-based model (ABM) is a modeling framework for complex systems by
117 simulating the dynamic interactions between automatic decision-making agents and
118 between these agents and the environment in a distributed micro level (Janssen and
119 Ostrom, 2006). As the warning responses are related to a learning process, and also to
120 personal flood experience and risk perception, ABM is suitable for understanding the
121 dynamic processes through simulating the individual decision-making (Anshuka et al.,
122 2022). Additionally, ABM can describe the spatially explicit social-hydrological
123 processes, such as the dissemination of warning information, the selection of
124 evacuation routes, and the distribution of flash flood inundation (Sivapalan and
125 Bloeschl, 2015). Thus, ABM is an effective tool for simulating the people's response
126 processes to flash flood warnings (Du et al., 2017; Yang et al., 2018; Zhuo and Han,
127 2020).

128 The aim of this study is to propose a method for determining the threshold of
129 issuing warnings (called warning threshold hereafter) based on the people's response
130 process simulation. A process-based ABM is developed to simulate people's response
131 processes to flash flood warnings (section 2.1). A simulation chain of "rainstorm
132 probability forecasting - decision on issuing warnings - warning response processes"
133 is conducted to determine the warning threshold based on the ABM (section 2.2).
134 Liulin Town in China is selected as a case study to demonstrate the proposed method,
135 and to provide valuable insights into the determination of warning threshold for
136 improving the effectiveness of flash flood warnings.



137 **2. Methodology**

138 **2.1. An ABM development for simulating people's response** 139 **processes to flash flood warnings**

140 To simulate the people's response processes to flash flood warnings (i.e.,
141 including the receiving warnings, the making evacuation decisions, the implementing
142 evacuation, and the being submerged by flash floods/the reaching shelters), an ABM
143 is developed by coupling social and natural sub-systems.

144 **2.1.1. Agents and their environments in the ABM**

145 There are two types of agents in the ABM: resident and authority. The resident
146 agents refer to the people threatened by flash floods. After receiving flash flood
147 warnings, the agents will decide whether and when to evacuate. If they decide to
148 evacuate, they will move along the roads towards the shelters. After issuing the
149 warnings, the flash flood will occur and might wash away the agents who have not
150 successfully arrived at shelters. The probability of casualties can be estimated based
151 on the velocity and the depth of the flash flood. The authority agents represent the
152 local authorities that mandate to prevent the flash flood disasters.

153 The environment in the ABM are the residences, road networks, shelters, and
154 floodwater. The residence agents are initially randomly distributed in the residences.
155 The resident agents who have decided to evacuate will move along the road network
156 instead of freely moving within the ABM area. The shelters are the destinations for
157 evacuation. The flash flood water not only affects the evacuation decisions and
158 behaviors of the resident agents but also causes casualties to the resident agents.

159 **2.1.2. Sub-modules of the ABM**

160 *Early warning sub-module.* Early warning sub-module simulates the process of
161 issuing warnings. Owing to the uncertainties of flash flood forecasting, there are
162 multiple stages of warning in a warning system. Rainstorm red, ready-to-evacuate,
163 and immediate-evacuation warnings are successively issued in the ABM. The times of
164 issuing these three warnings are determined by three parameters: lead time of
165 rainstorm red warning (indicated as *lead-time-w1*), ready-to-evacuate warning
166 (indicated as *lead-time-w2*), and immediate-evacuation warning (indicated as
167 *lead-time-w3*).

168 *Social sub-module.* Social sub-module simulates the people's psychological and



169 behavioral response processes to the warnings. The j -th agent¹ will decide to
170 evacuate when his/her overall evacuation intention (S_j , $S_j \in [0, 3]$) exceeds a
171 threshold, τ , or the water depth near him/her exceeds a threshold, EDT . There are
172 two components in S_j : evacuation intention arising from receiving warnings (S_j^W ,
173 $S_j^W \in \{1, 2, 3\}$), and evacuation intention arising from observing neighbors (S_j^N ,
174 $S_j^N \in [0, 1]$). The value of S_j^W is related to the socio-demographic and
175 socio-psychological attributes of the j -th agent (SSC_j) and the stages of the
176 receiving warning from the early warning sub-module (WT). The relationship can be
177 described by a random forest algorithm. The value of S_j^N equals to the proportion of
178 the j -th agent's neighbors who have decided to evacuate. The weights of the
179 influence of S_j^W and S_j^N on the S_j are represented by parameters α_j and β_j ,
180 respectively, and $\alpha_j + \beta_j = 1$. Finally, the overall evacuation intention of the j -th
181 agent at time t , $S_{j,t}$, is a linear combination of overall evacuation intention at time
182 $t-1$ ($S_{j,t-1}$) and current information. Learning rate, θ_j , measures the weight given
183 by the j -th agent to the obtained information at the current time. If the j -th agent
184 has decided to evacuate, he/she will walk along the shortest road network to the
185 shelters. His/her walking speed is estimated by the spatial-grid evacuation model
186 (SGEM) that has been developed by the City University of Hong Kong and Wuhan
187 University (Lo et al., 2004).

188 *Flood sub-module.* As flash flood can affect the people's evacuation behaviors
189 and cause casualties, the flash flood process is simulated in the flood sub-module. The
190 Hydrologic Engineering Center's River Analysis System (HEC-RAS) software is
191 gaining popularity due to its capabilities to simulate unsteady flow efficiently, and
192 identify and visualize flood-prone areas (Hicks and Peacock, 2005; Maidment, 2017).
193 The HEC-RAS model has been applied for flood forecasting and warning (Oleyiblo
194 and Li, 2010). And it has been adopted in our flood sub-module. The river geometries
195 such as centerlines, bank lines, and cross-sectional lines are the major parameters
196 proceeded in the HEC-RAS model to generate flood-prone areas. The spatiotemporal

¹ The agent refers to the resident agent by default



197 changes in the depth and velocity of flash floods are simulated by the HEC-RAS
198 model after the warnings.

199 **2.1.3. Casualty rate estimation module**

200 Based on the spatiotemporal distribution of the people outputted from the social
201 sub-module and the spatiotemporal distribution of floodwater outputted from the
202 flood sub-module, the casualty probability of an agent can be estimated via a logistic
203 regression equation as follows:

$$204 \quad f(z) = \frac{1}{1 + e^{15.48 - z}} \quad (1)$$

205 where $z = \beta_0 + \beta_1 \times h + \beta_2 \times u$, $\beta_0 = -12.37$, $\beta_1 = 22.036$, $\beta_2 = 11.517$. The flood
206 water depth is represented by h ($h \in [0.28, 0.85]$ (m)), and the flood water velocity
207 is denoted by u ($u \in [0.50, 2.00]$ (m/s)). The j -th agent is taken as casualty if the
208 h exceeds 0.85 m or u exceeds 2.00 m/s around him/her. The casualty rate is
209 estimated as the proportion of the casualties. A detail description of the ABM can be
210 retrieved from Zhang et al. (2024)

211 **2.1.4. A surrogate model development for the ABM**

212 Due to the complexity of the ABM, running this model once requires a
213 significant amount of time (Confalonieri et al., 2010). To simulate multiple flash flood
214 events, it is necessary to improve the computational efficiency of the ABM. Thus, a
215 Bayesian method developed by Oakley and O'Hagan (2004) is used to develop a
216 Gaussian process (GP) emulation as a surrogate model of the ABM. The GP
217 emulation can simulate the warning response processes more efficiently than the
218 original ABM (O'Hagan, 2006). In general, the GP emulation can be represented by
219 an equation: $D = f_{GP}(\mathbf{x})$ where D is the casualty rate at the end of the simulation
220 and \mathbf{x} are a set of parameters of the ABM.

221 A global sensitivity analysis of the ABM reveals that the weight of warning
222 influence, α , is the most sensitive parameter for the casualty rate (Zhang et al.,
223 2024). Furthermore, rainfall, P , is the driving factor causing flash floods. Therefore,
224 if there is a flash flood disaster and its corresponding warnings are issued, the ABM
225 can be simplified into a two-parameter surrogate model: $D = f_{GP}^2(\alpha, P)$. If there is a
226 flash flood disaster and no warning is issued, the ABM can be simplified into a
227 one-parameter surrogate model: $D = f_{GP}^1(P)$.



228 **2.2. Simulation chain of "rainstorm probability forecasting -** 229 **decision on issuing warnings - warning response processes"**

230 **2.2.1. Simulation of the rainstorm probability forecasting**

231 Flash floods often occur if there are sufficient rainstorms in a small basin over a
232 few hours (Collier, 2007; Younis et al., 2008). As the total flood generation and
233 routing time is very short, flash flood warnings have to be dependent on the rainstorm
234 forecasting for an enough lead time (Zhai et al., 2018). Therefore, the rainstorm
235 forecasting determines the flash flood warning decisions. The probabilistic forecasting
236 is preferred over the deterministic one as it considers forecasting uncertainties and it
237 is beneficial for rational decisions (Krzysztofowicz, 2001). A random probabilistic
238 forecasting generator based on Ambühl (2010) is employed to forecast the probability
239 distribution of rainfall as follows:

$$240 \quad F \sim N(P + N(\mu_{PA}, \sigma_{PA}^2), N(\mu_{PP}, \sigma_{PP}^2)) \quad (2)$$

241 where F is the forecasted rainfall, $N(\cdot)$ is the Gaussian distribution, P is the
242 actual rainfall, $N(\mu_{PA}, \sigma_{PA}^2)$ reflects the forecasting accuracy, and $N(\mu_{PP}, \sigma_{PP}^2)$
243 reflects the forecasting precision. Although Ambühl (2010) used the gamma
244 distribution to simulate the forecasting precision, the Gaussian distribution can help
245 improve the interpretability of the results. Negative $N(\mu_{PP}, \sigma_{PP}^2)$ is truncated to
246 1.0×10^{-6} to eliminate the negative values of variance.

247 We set $\mu_{PA}=0$ assuming the unbiased forecasting according to Sawada et al.
248 (2022). If the mean of the F (i.e., $P+N(0, \sigma_{PA}^2)$) is taken as the forecasting
249 tendency value, the accuracy of the forecasting tendency value will be reflected by
250 σ_{PA} . The variance of the F (i.e., $N(\mu_{PP}, \sigma_{PP}^2)$) determines the band-width of the
251 F . The larger $N(\mu_{PP}, \sigma_{PP}^2)$, the greater the band-width value of the F . The
252 variance of the forecasting values is determined by μ_{PP} , while the variance of the
253 variance of the forecasting values is determined by σ_{PP} .

254 **2.2.2. Simulation of the decision on issuing warnings**

255 There is a damage threshold, δ . If the P exceeds this threshold, flash flood
256 disasters will occur and cause damages. The probabilistic forecasting system can
257 provide the probability that the forecasted rainfall exceeds the δ (i.e., the
258 probability of flash flood disasters, denoted by $Prob$). If the $Prob$ is larger than a



259 preset threshold, λ , the warning administrators will issue the warnings. Thus, the λ
 260 is the warning threshold. The warning outcomes are dependent on a contingency table
 261 (shown in **Table 1**). The outcomes are dependent on two conditions: first, whether the
 262 $Prob$ is above the λ or not (i.e., whether to issue warnings or not); and second,
 263 whether the P exceeds the δ or not (i.e., whether to occur a flash flood disaster or
 264 not). The interplay of the two conditions leads to four warning outcomes: true
 265 negative (no warning), false negative (missed event), false positive (false warning),
 266 and true positive (successful warning). The missed events and the false warnings are
 267 collectively taken as failed warnings here.

268 **Table 1.** Contingency table defining the warning outcomes ^a

	$P < \delta$	$P \geq \delta$
$Prob < \lambda$	True negative (no warning) <i>0</i>	False negative (missed event) <i>Damage</i>
$Prob \geq \lambda$	False positive (false warning) <i>Cost</i>	True positive (successful warning) <i>Cost + residual damage</i>

269 ^a Costs and damages associated with each outcome. And they are highlighted in italics.

270 2.2.3. Simulation of the warning response processes

271 According to the four warning outcomes in **Table 1**, the warning response
 272 processes are simulated by the surrogate model of the ABM for estimating the
 273 casualty rate, D . If the warning outcome is true negative or false positive, the
 274 casualty rate is negligible as the actual rainfall, P , is smaller than the damage
 275 threshold, δ . It should be noted that false positive can cause opportunity cost as
 276 there are behavior responses to the warnings (i.e., evacuation behaviors). As this study
 277 only focuses on the casualty rate, the opportunity cost has been ignored. If the
 278 warning outcome is false negative, there is a flash flood disaster but no warning is
 279 issued. In this case, the one-parameter surrogate model (i.e., $D = f_{GP}^1(P)$) is
 280 employed to simulate the warning response processes for estimating the casualty rate.
 281 If the warning outcome is true positive, there is a flash flood disaster and its
 282 corresponding warnings are issued. The casualty rate is mitigated by evacuation. The
 283 two-parameter surrogate model (i.e., $D = f_{GP}^2(\alpha, P)$) is used to simulate the warning
 284 response processes for estimating the casualty rate. In general, the casualty rate can be
 285 described by the following equation:

$$286 \quad D = \begin{cases} 0 & \text{for true negative or false positive} \\ f_{GP}^1(P) & \text{for false negative} \\ f_{GP}^2(\alpha, P) & \text{for true positive} \end{cases} \quad (3)$$



287 We assume that past warning outcomes affect people’s trust levels in the
 288 warnings. Existing studies have found that the recent false warning ratio undermines
 289 people’s trust levels in the warnings and their preparedness actions (Jauernic and Van
 290 den Broeke, 2017; LeClerc and Joslyn, 2015; Lim et al., 2019; Ripberger et al., 2015).
 291 It is reasonable to assume that people’s past experiences with successful (or failed)
 292 warnings increase (or decrease) their trust levels in the warnings. A person’s trust
 293 level in the warnings can be described by the parameter α representing the weight
 294 assigned to the warning information. Therefore, α after experiencing a flash flood
 295 at the $t+1$ time can be described by the following equation:

$$296 \quad \alpha(t+1) = \begin{cases} \alpha(t) & \text{for true negative} \\ \alpha(t) - \chi_{FN} & \text{for false negative} \\ \alpha(t) - \chi_{FP} & \text{for false positive} \\ \alpha(t) + \chi_{TP} & \text{for true positive} \end{cases} \quad (4)$$

297 where χ_{FN} , χ_{FP} , and χ_{TP} are increments of α for false negative, false positive,
 298 and true positive, respectively. If α is larger than one, it is truncated to one. If α
 299 is smaller than zero, it is truncated to zero.

300 2.2.4. Performance metrics of the warning

301 Three metrics are used to evaluate the warning performance: the relative
 302 casualty rate (D_r), missed event ratio (MER), and false warning ratio (FWR). The
 303 D_r is defined as:

$$304 \quad D_r = \frac{D_w}{D_n} \quad (5)$$

305 where D_w is the average casualty rate of multiple flash floods if there is a flash flood
 306 warning. And the casualty rate of each flash flood can be estimated by equation (3).
 307 D_n is the average casualty rate of multiple flash floods if there is no flash flood
 308 warning in place (i.e., the casualty rate is dependent only on the natural variability).
 309 The casualty rate of each flash flood can be estimated by the following equation (6).

$$310 \quad D_n = \begin{cases} 0 & \text{if } P < \delta \\ f_{GP}^1(P) & \text{if } P \geq \delta \end{cases} \quad (6)$$

311 The lower the value of D_r , the more effective the flash flood warning is. If the
 312 objective of flash flood warning is the minimizing the casualties, the optimal warning
 313 threshold is the threshold where the D_r is the lowest.



314 Besides D_r , the MER and FWR are used to evaluate the performance of the
315 flash flood warning. They are defined by equations (7) and (8):

316
$$MER = \frac{O_{FN}}{O_{TP} + O_{FN}} \quad (7)$$

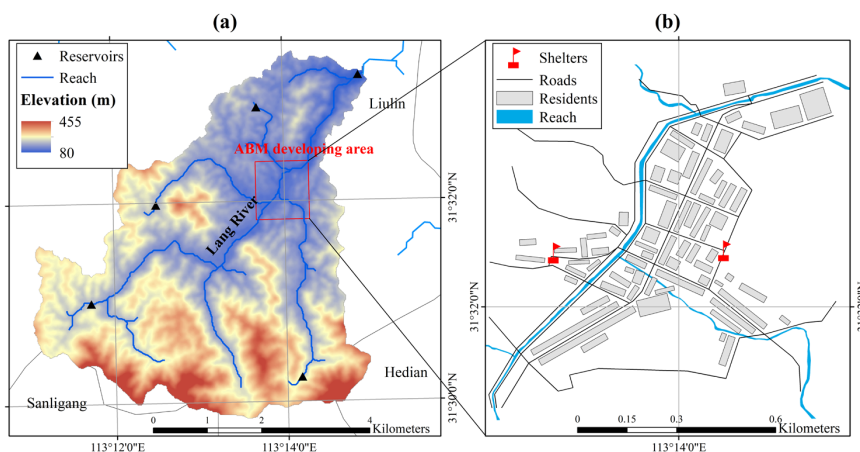
317
$$FWR = \frac{O_{FP}}{O_{FP} + O_{TP}} \quad (8)$$

318 where O_{FN} , O_{TP} , O_{FP} are the total number of false negative, true positive, and
319 false positive events, respectively.

320 **3. Case study**

321 **3.1. Study area**

322 Liulin Town located in Suixian Country, Hubei Province, China was selected as
323 our study area. The Lang River goes through Liulin Town as shown in **Figure 1(a)**
324 and the red rectangular box indicates the location of the town. The average annual
325 rainfall is 1,100 mm. Rainfall is unevenly distributed throughout the year, and mainly
326 concentrates from June to August. The upstream valley of Liulin Town is wider than
327 that of the downstream. And this river geomorphology hinders flood discharge and
328 easily causes the flash flood disaster when a rainstorm occurs. Residences in the town
329 are located on both sides of Langhe River. In the prevention and control map of flash
330 flood disasters in Suixian County, two communities in Liulin Town are listed as
331 high-risk and relatively high-risk areas. Especially, an extreme rainstorm with a
332 volume of 503 mm from 2:00 a.m. to 9:00 a.m. on August 12, 2021 (hereafter called
333 the 8.12 event) caused a severe flash flood disaster in the town. Unfortunately, 21
334 people were dead and four people were still missing in this disaster although flash
335 flood warnings had been issued (Wei, 2021). Exploring the way to determine the
336 threshold of issuing flash flood warnings in the town will provide valuable
337 information on flash flood disaster prevention for reducing the casualties.



338

339 **Figure 1.** Location of the (a) Lang River Basin and (b) Liulin Town

340 **3.2. Setting of the ABM**

341 To set up the environment of the ABM, the residences and road network (see
342 **Figure 1**) were imported into the model after processing a digital archive (i.e., World
343 Imagery Wayback). To prevent evacuation across the river, two shelters were set up at
344 high place on both sides of the Langhe River. And they should not be submerged by
345 floods. The parameters of the ABM were set according to calibration, empirical data,
346 and related literature (see **Table 2**). The lead time of the three stages of warning and
347 evacuation depth threshold were parameterized from the two-month surveying
348 expertise and experience in the study area. The three hyperparameters of the random
349 forest model were calibrated by the empirical data from our survey. A sampling
350 without replacement was conducted on the empirical data and the sample was used to
351 assign the initial SSC values of the agents. The random forest model calibration, the
352 survey, and the method of assigning SSC values were detailed in Zhang et al. (2024).
353 The values of θ_j and p_j of the j -th agent were sampled from the Gaussian
354 distributions according to the exiting literature (Du et al., 2017). $S_j = 2$ is set to
355 indicate no decision making on evacuation for the j -th agent in the empirical data
356 while $S_j > 2$ means the evacuation decision of the agent. Hence, the value of τ
357 was set to 2. A global sensitivity analysis has been performed to explore the relative
358 impacts of these parameters on the casualty rate and can be retrieved from Zhang et al.
359 (2024).

360



361 **Table 2.** Fixed ABM parameters

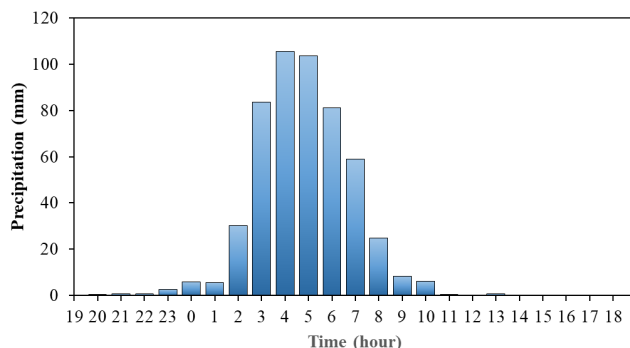
Sub-module	Parameters	Symbol	Values	Remark
Early warning	Lead time of rainstorm red warning	<i>lead-time-w1</i>	120 min	Author estimation ^a
	Lead time of ready-to-evacuate warning	<i>lead-time-w2</i>	60 min	Author estimation ^a
	Lead time of immediate-evacuation warning	<i>lead-time-w3</i>	30 min	Author estimation ^a
Random forest	Number of trees	<i>ntree</i>	500	Calibration
	Number of candidate variables	<i>mtry</i>	6/1/6 ^b	Calibration
	Minimum size of nodes	<i>nodesize</i>	10/1/10 ^b	Calibration
	Socio-demographic and socio-psychological characteristics of resident agents	<i>SSC</i>		Empirical data
Opinion dynamics	Learning rate	θ	0.5 (0.1) ^c	Literature reference (Du et al., 2017)
	Probability of receiving early warnings	P	0.1 (0.1) ^c	Literature reference (Du et al., 2017)
	Evacuation threshold	τ	2	Empirical data
Others	Visual range	<i>VR</i>	40 m	Literature reference (Wu et al., 2022)
	Evacuation depth threshold	<i>EDT</i>	0.28 m	Author estimation ^a

362 ^aThese estimations are from the two-month surveying expertise and experience of the authors
 363 in the study area. ^b $x_1/x_2/x_3$ indicates the values of the factors are x_1 , x_2 , and x_3 for the
 364 rainstorm red, the ready-to-evacuate, and the immediate-evacuation warnings, respectively. ^c
 365 x_1 (x_2) indicates the values of the factors are sampled from a normal distribution with mean
 366 value of x_1 and variance of x_2

367 The flood-module of the ABM was formed by a two-dimensional (2D)
 368 hydrodynamic model in the Langhe River Basin through HEC-RAS. Terrain
 369 information was obtained from the digital elevation model (DEM) at a spatial
 370 resolution of 12.5 m provided by the Advanced Land Observing Satellite (ALOS).
 371 Cells with size of 30 m were generated within the 2D flow areas. The Manning's
 372 coefficient was set to a unified comprehensive value of 0.045. The upstream boundary
 373 condition was set as the rainstorm process. The hyetograph was selected by the
 374 measured rainfall process of the 8.12 event. Specifically, the hourly rainfall was
 375 greater than 30.0 mm from 2:00 to 7:00 on August 11, 2021 and the 6-h rainfall was
 376 up to 462.6 mm (see **Figure 2**). The 6-h rainfall process was input into the HEC-RAS
 377 as the hyetograph. As Baiguo River reservoir is in the outlet, the downstream
 378 boundary condition was set as the normal water level of the reservoir. The



379 spatiotemporal changes in the depth and velocity of flash floods were exported after
380 running the model at a temporal interval of 2 min and spatial resolution of 12.5 m.



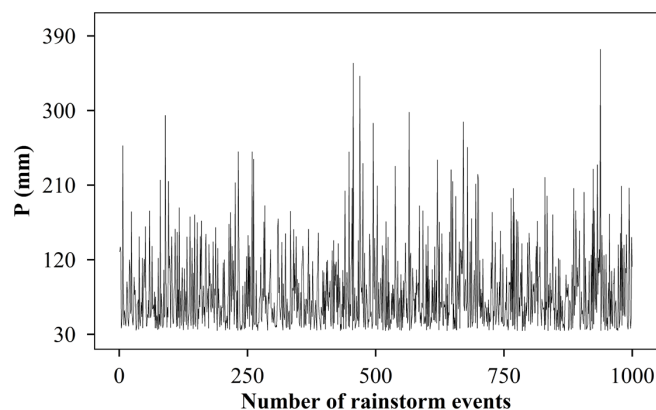
381

382 **Figure 2.** The rainfall process from 19:00 on August 11 to 19:00 on August 12, 2021
383 of Liulin Meteorological Station

384 The ABM was run by covering the processes from issuing warnings to flash
385 flood at a time step of 1 min and spatial resolution of 9.6 m. And 500 agents were
386 assumed to be involved in the simulations. Due to the inherent randomness of the
387 ABM, the averages of the outputs from the repeating 1,000 times for running the
388 ABM were obtained to ensure stable outputs.

389 3.3. Rainfall data

390 A series of rainfall data was imported into the ABM for simulating a series of
391 possible flash flood disasters. Synthetic rainfall series are required to ensure the
392 representative of the extreme events. The annual maximum 6-h rainfall, P , was
393 assumed to follow the Pearson III distribution. Its values of mean and C_v in the
394 basin above Liulin Town were estimated to be 80 mm and 0.6, respectively, according
395 to Atlas of Statistical Parameters of rainstorm in Hubei Province (2008). C_s / C_v was
396 taken as 3.5 in Hubei Province. 1,000 synthetic rainstorm events were randomly
397 generated by the Pearson III distribution, and the result was shown in **Figure 3**.



398
 399 **Figure 3.** 1,000 synthetic series of rainstorm events

400 **3.4. Model test experiments**

401 To determine the warning threshold under different forecasting skills for
 402 minimizing the relative casualty rate, three possible values of each of the three
 403 parameters (i.e., σ_{PA} , μ_{PP} , and σ_{PP}) were prepared to reflect different forecasting
 404 skills (see **Table 3**) and their interactive effects on the determination of warning
 405 threshold were tested. Rainstorm red warning is the highest level of meteorological
 406 risk warning in the mainland of China. When the rainstorm red warning is issued,
 407 floods tend to cause damage and the residents in flood risk area are advised to
 408 evacuate (Wang et al., 2020). If the 6-hour rainfall is up to 150 mm, the rainstorm red
 409 warning will be issued (Shanghai Meteorological Bureau, 2019). Thus, the value of
 410 δ was taken as 150 mm in the case study.

411 **Table 3.** Model test experiment for determining the warning threshold under different
 412 forecasting skills

Parameters	Symbol	Values
The accuracy of the forecasting tendency value	σ_{PA}	{0.05, 0.10, 0.15}
The variance of the forecasting values	μ_{PP}	{0.0, 0.1, 0.2}
The variance of the variance of the forecasting values	σ_{PP}	{0.0, 0.1, 0.2}
Damage threshold	δ	150 mm
Increment of α for false negative	χ_{FN}	0.1
Increment of α for false positive	χ_{FP}	0.1
Increment of α for true positive	χ_{TP}	0.1

413 Besides the uncertainties of the forecasting, there are uncertainties in people's
 414 response processes to the uncertain forecasting. To determine the warning threshold
 415 under different forecasting skills and tolerance levels of the failed warnings, the



416 warning threshold was determined under different σ_{PA} and combinations of
 417 parameters related to the increments of α (i.e., χ_{FN} , χ_{FP} , and χ_{TP}) through Exp1
 418 in **Table 4**, and under different μ_{PP} and combinations of parameters related to the
 419 increments of α through Exp 2 in **Table 4**. The higher the χ_{FN} and χ_{FP} , the
 420 lower the tolerance levels of the people towards the missed event and the false
 421 warnings, respectively.

422 **Table 4.** Model test experiment for determining the warning threshold under different
 423 forecasting skills and tolerance levels of the failed warnings

Parameters	Symbol	Values	
		Exp1	Exp2
The accuracy of the forecasting tendency value	σ_{PA}	{0.05, 0.10, 0.15}	0.075
The variance of the forecasting values	μ_{PP}	0.15	{0.0, 0.1, 0.2}
The variance of the variance of the forecasting values	σ_{PP}	0.075	0.075
Damage threshold	δ	150 mm	150 mm
Increments of α for false negative, false positive, and true positive	$\chi_{FN}/\chi_{FP}/\chi_{TP}$	{0.1/0.1/0.1, 0.8/0.8/0.1, 0.8/0.1/0.1, 0.1/0.8/0.1}	{0.1/0.1/0.1, 0.8/0.8/0.1, 0.8/0.1/0.1, 0.1/0.8/0.1}

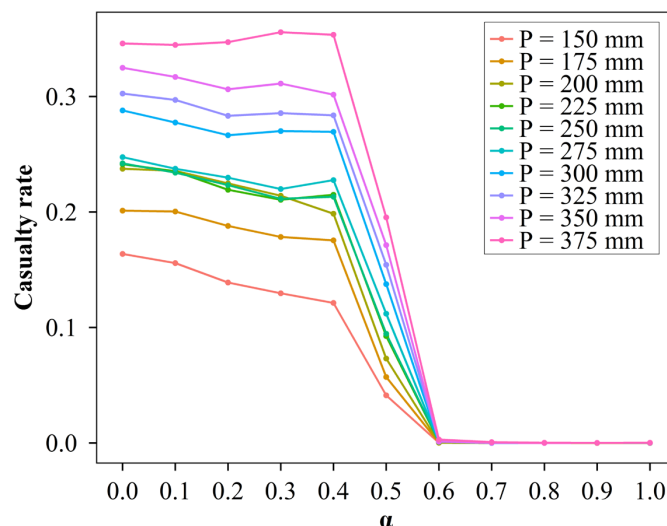
424 **4. Results and discussions**

425 **4.1. The casualty rate from people's response process simulation**

426 To determine the warning threshold based on the people's response process
 427 simulation, the ABM with different values of P and α were run to generate
 428 corresponding casualty rates, and these simulations were taken as sample data to train
 429 the GP emulation as a surrogate model of the ABM, as shown in **Figure 4**. And it has
 430 shown the variation of casualty rate with α under different P . There are three
 431 stages of change in the casualty rate as α increases regardless of P . When α
 432 increases from 0.0 to 0.4, the casualty rate slowly decreases; but as α continues to
 433 increase to 0.6, the rate of decline becomes faster. When α is greater than or equal
 434 to 0.6, everyone arrives at the shelters before the flash flood disaster arrives and there
 435 are no casualties regardless of P . This result implies that it is very important and
 436 effective to enhance people's trust levels in the warnings when people have similar
 437 trust levels in warning information and their neighbors. When people's trust in
 438 warning information decreases, their evacuation decisions will become more
 439 dependent on whether their neighbors are evacuating or not. In other words, the



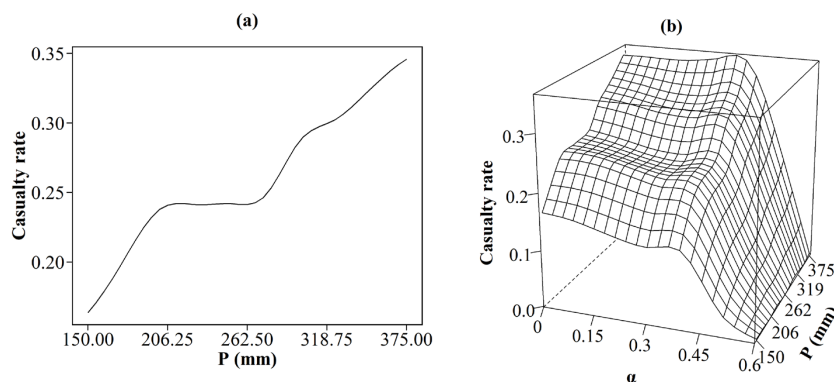
440 increase in the overall evacuation intention (S) of agents requires their neighbors to
441 take evacuation actions. However, taking evacuation actions requires the increase in
442 S in turn. Thus, waiting for others' evacuation ultimately leads to neither an increase
443 in S nor the implementation of evacuation actions.



444
445 **Figure 4.** The casualty rate under different values of P and α from ABM
446 simulations
447 Because the casualty rate is zero when α is greater than or equal to 0.6
448 regardless of P , the one-parameter and two-parameter GP emulations were trained
449 for α with a value less than 0.6 and the results were shown in **Figure 5**. The
450 training result for one-parameter GP emulation shows that there are also three stages
451 in the increase of casualty rate as P increases. When P increases from 150 to 200
452 mm, the casualty rate increases; but if P increases from 200 to 260 mm, the
453 casualty rate remains almost unchanged. When P exceeds 260 mm and continues to
454 increase, the casualty rate starts to increase again. This result indicates that there is
455 spatial heterogeneity of flood risk levels in the case study. It is necessary to classify
456 flood risk zones and distinguish water level or rainfall thresholds for triggering
457 evacuation according to different flood risk levels. The training result for
458 two-parameter GP emulation shows the complex responses of casualty rate to changes
459 in α and P . When α is less than 0.4, there are three stages of changes in the
460 casualty rate as P increases. As α increases from 0.4 to 0.6, the relationship
461 between P and casualty rate tends to be linearly positive, and the difference in



462 casualty rates under different P gradually reduces. This result means that the trust
463 level in the warnings becomes the dominant factor in determining the casualty rate
464 when the people's trust levels in the warnings and their neighbors are similar (i.e.,
465 when the value of α is the range of 0.4 to 0.6).



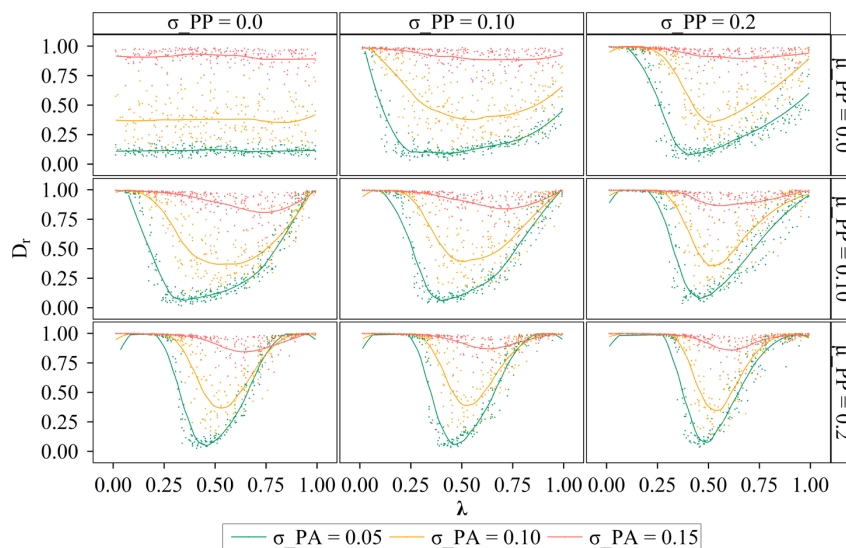
466
467 **Figure 5.** Trained (a) one-parameter and (b) two-parameter GP emulations for
468 casualty rate

469 **4.2. Determining the warning threshold under different** 470 **forecasting skills for minimizing casualties**

471 To determine the warning threshold under different forecasting skills for
472 minimizing casualties, 250-member Monte Carlo simulations were performed on the
473 simulation chain of "rainstorm probability forecasting - decision on issuing warnings -
474 warning response processes" by randomly perturbing the warning threshold, λ ,
475 under different values of parameters controlling the forecasting skills (see **Figure 6**).
476 Different rows represent different values of μ_{pp} , and there is a larger forecasting
477 variance in the sub-graph of the lower row. Similarly, there is a larger variance of the
478 forecasting variance in the sub-graph of the right column compared to the sub-graph
479 of the left column. The highest forecasting accuracy is represented by the green
480 curves, followed by the yellow curves, and finally the red curves. In all the sub-graphs,
481 there is the highest relative casualty rate in the red curves, followed by the yellow
482 curves, and finally the green curves. Therefore, the lower the forecasting accuracy,
483 the higher the relative casualty rate. The optimal warning threshold can be taken as the
484 value of λ where the relative casualty rate, D_r , is lowest. The optimal warning
485 thresholds are the lowest in the green curves, followed by the yellow curves, and



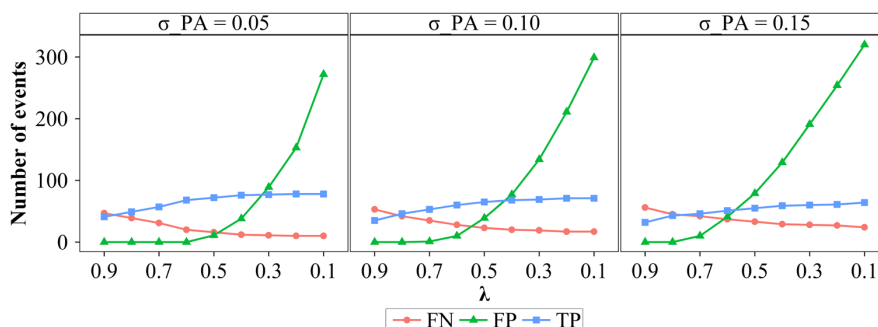
486 finally the red curves in all the sub-graphs. Thus, the lower the forecasting accuracy,
 487 the higher the optimal warning threshold. The reasons can be found in **Figure 7**. As
 488 the warning threshold decreases, the number of false warnings and successful
 489 warnings increases, and more warnings are issued. However, if the forecasting
 490 accuracy is low, the proportion of false warnings is higher than that of successful
 491 warnings among the additional warnings issued. For example, as the warning
 492 threshold decreases, the green curve for low forecasting accuracy rises faster than that
 493 for high forecasting accuracy. This means that if the forecasting accuracy is low, as
 494 the warning threshold decreases, the increase speed of false warnings is higher than
 495 that of successful warnings. In addition, when the warning threshold is less than 0.7,
 496 the green curve begins to rise rapidly for $\sigma_{PA} = 0.15$, while it does not start to rise
 497 rapidly until the warning threshold is less than 0.5 for $\sigma_{PA} = 0.15$. Therefore, when
 498 the forecasting accuracy is low, a high warning threshold should be set. As the
 499 forecasting accuracy increases, lowering the warning threshold can result in more
 500 successful warnings without significantly increasing false warnings, thereby
 501 improving the effectiveness of flash flood warnings.



502
 503 **Figure 6.** The relationship between the relative casual rate, D_r , and the warning
 504 threshold, λ , under different values of σ_{PA} , μ_{PP} , and σ_{PP} . Different rows and
 505 columns represent different values of μ_{PP} and σ_{PP} , respectively. Different colors



506 represent different values of σ_{PA} . Each dot shows the result of the individual Monte
 507 Carlo simulation



508
 509 **Figure 7.** The changes in the number of false negative, false positive, and true
 510 positive events as warning threshold decreases, λ under different values of σ_{PA} .
 511 The range of λ is reversed from 0.9 to 0.1

512 In terms of the impacts of the forecasting variance (see **Figure 6**), there is a
 513 larger forecasting variance and a higher relative casualty rate of three colored curves
 514 in the sub-graph of the lower row. Thus, the larger the forecasting variance, the higher
 515 the relative casualty rate. For the optimal warning threshold, the differences in the
 516 optimal warning thresholds of these three colored curves are smaller in the sub-graph
 517 of the lower row. For instance, as the forecasting variance increases, the optimal
 518 warning thresholds for the red curves decrease while the optimal warning thresholds
 519 for the green curves increase. This result means that the larger the forecasting
 520 variance, the lower the optimal warning threshold for low forecasting accuracy, while
 521 the larger the forecasting variance, the higher the optimal warning threshold for high
 522 forecasting accuracy. When the forecasting accuracy is at a low level, a large
 523 forecasting variance is actually beneficial for improving the forecasting skills. High
 524 forecasting skill means that more successful warnings and fewer false warnings are
 525 issued after lowering the warning threshold. Therefore, if the forecasting accuracy is
 526 at a low level, as the forecasting variance increases, the warning threshold can be
 527 lowered. On the contrary, if the forecasting accuracy is at a high level, as the forecast
 528 variance increases, increasing the warning threshold can significantly decrease the
 529 false warnings and improve the effectiveness of flash flood warnings. Finally, we
 530 focused on the impacts of the variance of the forecasting variance. Similar to the
 531 impacts of the forecasting variance, the larger the variance of the forecasting variance,



532 the higher the relative casualty rate. As the variance of the forecasting variance
533 increases, the optimal warning threshold tends to decrease for low forecasting
534 accuracy or to increase for high forecasting accuracy.

535 The impacts of the three parameters (i.e., σ_{PA} , μ_{PP} , and σ_{PP}) on the shape of
536 the relationship curve between D_r and λ can be analyzed as follows. As shown in
537 **Figure 6**, σ_{PA} determines the height of the curve, while μ_{PP} and σ_{PP} determine
538 the width of the curve. Specifically, as the forecasting accuracy increases, the
539 stationary point of the curve moves down and the curve becomes higher; as the
540 forecasting variance or the variance of the forecasting variance increases, the curve
541 becomes narrower. If the forecasting accuracy is high and the forecasting variance and
542 the variance of the forecasting variance are large, the curve will become high and
543 narrow, such as the green curve for $\mu_{PP} = 0.2$ and $\sigma_{PP} = 0.2$. And there is only a
544 low relative casualty rate near the optimal warning threshold in this green curve. Thus,
545 it is more important to determine the optimal warning threshold for minimizing
546 casualties if the forecasting accuracy is higher, and the forecasting variance and the
547 variance of the forecasting variance are larger.

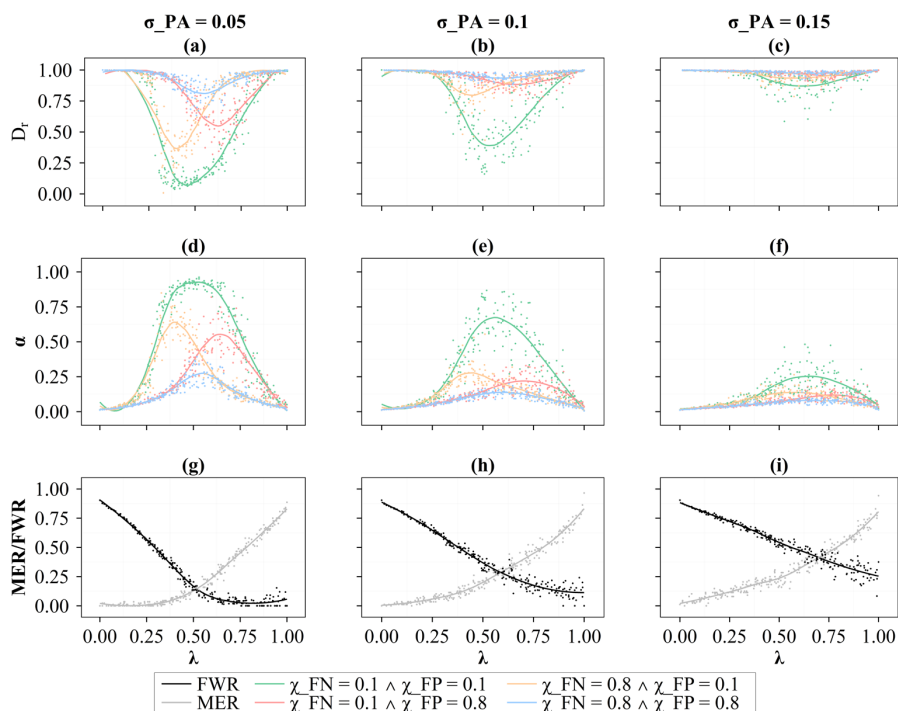
548 **4.3. Determining the warning threshold under different** 549 **forecasting skills and tolerance levels of the failed warnings for** 550 **minimizing casualties**

551 To determine the warning threshold under different forecasting skills and
552 tolerance levels of the failed warnings for minimizing casualties, the simulation chain
553 of "rainstorm probability forecasting - decision on issuing warnings - warning
554 response processes" was run with random values of λ under different σ_{PA} and
555 combinations of parameters related to the increments of α (i.e., χ_{FN} , χ_{FP} , and
556 χ_{TP}) (see **Figure 8**), and different μ_{PP} and combinations of parameters related to the
557 increments of α (i.e., χ_{FN} , χ_{FP} , and χ_{TP}) (see **Figure 9**). Owing to the similar
558 roles of μ_{PP} , and σ_{PP} , the effects of σ_{PP} on the determination of warning
559 threshold were not explored here. As shown in **Figure 8**, the optimal warning
560 thresholds for the yellow curves are the lowest. The yellow curves represent scenarios
561 that people's trust in warnings is sensitive to false negative events and people have a
562 low tolerance level for the missed events. To reduce the missed event ratio, the



563 warning threshold should be lowered (see **Figure 8g**). Therefore, the warning
564 threshold should be lowered for increasing people's trust levels in warnings and
565 reducing casualties if people have a lower tolerance level for the missed events.
566 Similarly, the warning threshold should be increased if the people's tolerance levels
567 for the false warnings become lower (see the red curves). And if the people's tolerance
568 for both the missed events and the false warnings decreases to the same level, the
569 optimal warning threshold remains almost unchanged, but the relative casualty rate
570 overall increases (see the blue curves). As for the relative casualty rate, the relative
571 casualty rates of the yellow curves are lower than those of the red curves. This result
572 suggests that compared to the missed events, the people's low tolerance levels for the
573 false warnings are less conducive to the effectiveness of flash flood warnings. As
574 shown in **Figure 7**, the number of false warnings is greater than the number of missed
575 events in general. Therefore, if the people's tolerance levels for the false warnings is
576 low, their trust levels in warnings are more likely to decrease, leading to the effects of
577 "cry wolf".

578 By comparing **Figure 8a** and **Figure 8b**, the overall height of the curves
579 decreases when the forecasting accuracy decreases, as discussed in the last paragraph
580 of section 4.2. However, compared to green curve, the heights of other curves
581 decrease more significantly. And the relative casualty rates are high at any warning
582 threshold (i.e., $D_r > 0.75$) except for the green curve when the σ_{PA} increases from
583 0.05 to 0.1. It is more pronounced when the σ_{PA} further increases to 0.15. Therefore,
584 as the forecasting accuracy decreases, the benefits gained by adjusting the warning
585 threshold based on the people's tolerance levels of the failed warnings decreases. In
586 other words, no matter how the warning threshold is adjusted, the relative casualty
587 rate is high and the effectiveness of warning is at a low level.



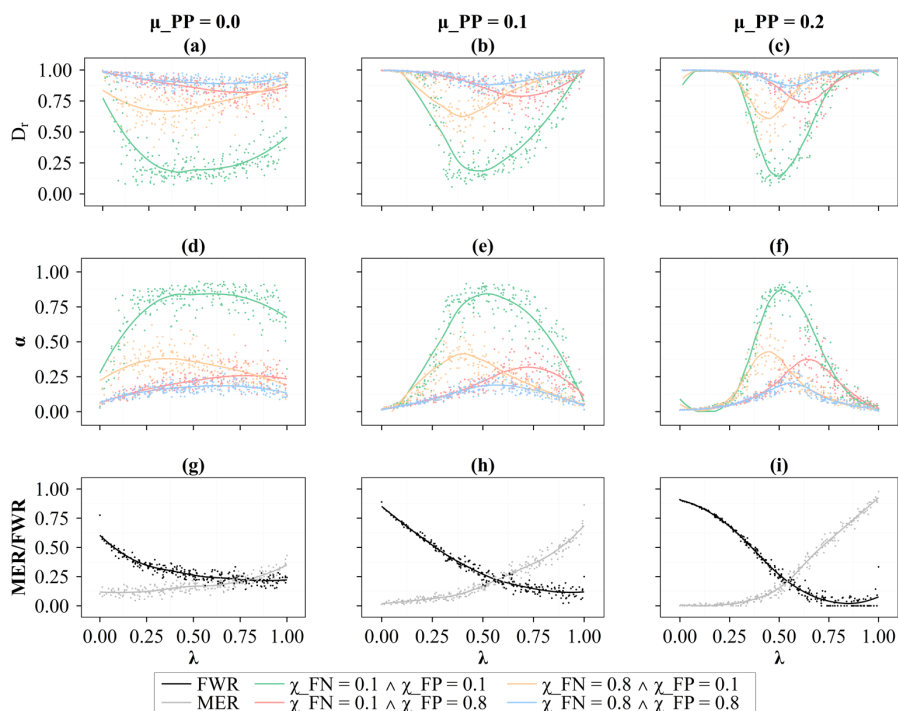
588
 589 **Figure 8.** (a-c) The relationship between the warning threshold, λ and the relative
 590 casualty rate, D_r under different σ_{PA} and combinations of parameters related to the
 591 increments of α (i.e., χ_{FN} , χ_{FP} , and χ_{TP}). (d-f) Same as (a-c) but for
 592 time-averaged α . (g-i) The relationship between the warning threshold, λ , and the
 593 false warning ratio, FWR , and the missed event ratio, MER , under different σ_{PA} .
 594 Each dot shows the result of the individual Monte Carlo simulation

595 In terms of the effects of the forecasting variance and the tolerance levels of the
 596 failed warnings on the determination of warning threshold as shown in **Figure 9**, the
 597 warning threshold should be decreased if people have a lower tolerance level for the
 598 missed events, and vice versa. And compared to the missed events, the people's low
 599 tolerance levels for the false warnings are less conducive to the effectiveness of flash
 600 flood warnings. These findings are consistent with the results in **Figure 8**.
 601 Furthermore, we find that the difference in the optimal warning thresholds of these
 602 colored curves decreases as the forecasting variance increases as shown in **Figure**
 603 **9a-Figure 9c**. As discussed in the last paragraph of section 4.2, the curve becomes
 604 narrower as the forecasting variance increases. If the width of the curves decreases,
 605 the difference between their optimal warning thresholds will also decrease. Therefore,



606 as the forecasting variance increases, the difference in the optimal warning thresholds
607 of these curves will decrease, and the adjustment space for the warning threshold
608 based on the people's tolerance levels will also decrease.

609 If the green curve represents the result of the baseline scenario where both χ_{FN}
610 and χ_{FP} equal 0.1, increment of the values of χ_{FN} and χ_{FP} (i.e., lowering
611 tolerance levels for the missed events and the false warnings) will result in a series of
612 curves, and these curves will be enveloped by the green curve in **Figure 9**. Therefore,
613 only when the green curve is high enough, can the relative casualty rate of this series
614 of curves be low enough, and the effectiveness of flash flood warnings be sufficiently
615 improved. And only when the green curve is wide enough, can the difference in the
616 optimal warning threshold for this series of curves be large enough, and there can be
617 enough room for adjustment the warning threshold. In summary, by increasing the
618 height and width of the green curve, the adjustable room for the warning threshold
619 will be larged and the effectiveness of flash flood warnings will be improved. As the
620 forecasting accuracy increases, the green curve becomes higher. And as the
621 forecasting variance decreases, the green curve becomes wider. Therefore, under the
622 premise of improving the forecasting skills (i.e., increasing forecasting accuracy and
623 decreasing forecasting variance), adjusting the warning threshold based on the
624 people's tolerance levels of the failed warnings is one of the ways to improve the
625 effectiveness of flash flood warnings.



626
 627 **Figure 9.** (a-c) The relationship between the warning threshold, λ and the relative
 628 casualty rate, D_r under different μ_{PP} and combinations of parameters related to the
 629 increments of α (i.e., χ_{FN} , χ_{FP} , and χ_{TP}). (d-f) Same as (a-c) but for
 630 time-averaged α . (g-i) The relationship between the warning threshold, λ , and the
 631 false warning ratio, FWR , and the missed event ratio, MER , under different μ_{PP} .
 632 Each dot shows the result of the individual Monte Carlo simulation

633 5. Conclusions

634 A method has been proposed to determine the warning threshold for minimizing
 635 casualties based on the people's response process simulation. A process-based ABM
 636 was developed to simulate people's response processes to flash flood warnings. A
 637 simulation chain of "rainstorm probability forecasting - decision on issuing warnings -
 638 warning response processes" was conducted to determine the warning threshold based
 639 on the ABM. The main conclusions are as follows.

640 The casualty rate is jointly controlled by the warning information source and
 641 precipitation. If the people's trust levels in official warnings are below a certain
 642 threshold, precipitation is the dominant factor in controlling the casualty rate. If the



643 people have a similar level of trust in official warnings and neighbor behaviors, the
644 credibility of the warning information source is the dominant factor in controlling the
645 casualty rate.

646 The warning threshold has been determined under different forecasting skills for
647 minimizing casualties. The lower the forecasting accuracy, the higher the optimal
648 warning threshold. And the larger the forecasting variance or the variance of the
649 forecasting variance, the higher (lower) the optimal warning threshold for high (low)
650 forecasting accuracy. Furthermore, the impact pattern of forecasting skills on the
651 shape of the relationship curve between the relative casualty rate and the warning
652 threshold has been revealed: the curve becomes higher as the forecasting accuracy
653 increases, and the curve becomes narrower as the forecasting variance or the variance
654 of the forecasting variance increases.

655 The warning threshold has been determined under different forecasting skills and
656 tolerance levels of the failed warnings for minimizing casualties. The warning
657 threshold should be decreased (increased) if people have a lower tolerance level for
658 the missed events (the false warnings). However, if the forecasting accuracy is low
659 and the forecasting variance is large, the space for adjusting the warning threshold is
660 limited, and no matter how the warning threshold is adjusted, the casualty rate
661 remains at a high level, and the effectiveness of flash flood warnings is limited.
662 Therefore, under the premise of improving the forecasting skills, adjusting the
663 warning threshold based on the people's tolerance levels of the failed warnings is one
664 of the ways to improve the effectiveness of flash flood warnings.

665 Although our study provides valuable insights into the determination of warning
666 threshold for minimizing casualties, it should be noted that there are some
667 assumptions underlying the simulation method. The parameters of ABM were
668 assumed to be time invariant except for α . Updating the values of these parameters
669 based on past warning outcomes will provide more information for determining the
670 warning threshold. The hyetograph was selected as the measured rainfall process of
671 the 8.12 event. More uneven hyetographs should be taken in the flash flood
672 simulation, and the impact of hyetograph on the warning threshold determination can
673 be explored in further research. The casualty rate caused by pluvial floods varies with
674 different spatial distribution of rainfall. The people's trust levels in the warnings were
675 assumed to be only affected by the past warning outcomes. There are other factors
676 (e.g., social education and government authority) that should be incorporate into the



677 estimation of the people's trust levels. Therefore, there are still works can be done in
678 the future.

679 **Code availability**

680 The code that supports the findings of this study is available from the
681 corresponding author upon reasonable request.

682 **Date availability**

683 Data will be made available on request.

684 **Author contribution**

685 Ruikang Zhang: Conceptualization, Formal analysis, Methodology, Writing –
686 original draft, Visualization, Funding acquisition. Dedi Liu: Conceptualization, Data
687 curation, Formal analysis, Funding acquisition, Methodology, Supervision, Writing -
688 review & editing. Lihua Xiong: Project administration, Supervision. Jie Chen: Data
689 support, Methodology, Writing - review & editing. Hua Chen: Validation, Writing -
690 review & editing, Supervision. Jiabo Yin: Validation, Writing - review & editing. All
691 authors contributed to the interpretation of the results and to the text.

692 **Competing interests**

693 The authors declare that they have no conflict of interest.

694 **Disclaimer**

695 Publisher's note: Copernicus Publications remains neutral with regard to
696 jurisdictional claims in published maps and institutional affiliations.

697 **Acknowledgments**

698 The authors gratefully acknowledge the financial support from National Key
699 Research and Development Project of China (2022YFC3202803), the National
700 Natural Science Foundation of China (52379022), and the Open Innovation
701 Foundation funded by ChangJiang Survey, Planning, Design and Research Co., Ltd
702 (CX2021K04).

703



References:

- 704
705 Ambühl, J.: Customer oriented warning systems, Veröffentlichung MeteoSchweiz Nr. 84, 1-86, 2010.
706 Anshuka, A., van Ogtrop, F. F., Sanderson, D., and Leao, S. Z.: A systematic review of agent-based
707 model for flood risk management and assessment using the ODD protocol, *Nat. Hazards*, 112,
708 2739-2771, <https://doi.org/10.1007/s11069-022-05286-y>, 2022.
709 Bodoque, J. M., Diez-Herrero, A., Amerigo, M., Garcia, J. A., and Olcina, J.: Enhancing flash flood
710 risk perception and awareness of mitigation actions through risk communication: A pre-post survey
711 design, *J. Hydrol.*, 568, 769-779, <https://doi.org/10.1016/j.jhydrol.2018.11.007>, 2019.
712 Boelee, L., Lumbroso, D. M., Samuels, P. G., and Cloke, H. L.: Estimation of uncertainty in flood
713 forecasts-A comparison of methods, *J. Flood Risk Manag.*, 12, e12516,
714 <https://doi.org/10.1111/jfr3.12516>, 2019.
715 Borga, M., Comiti, F., Ruin, I., and Marra, F.: Forensic analysis of flash flood response, *Wiley*
716 *Interdiscip. Rev.-Water*, 6, e1338, <https://doi.org/10.1002/wat2.1338>, 2019.
717 Cheng, W.: A review of rainfall thresholds for triggering flash floods, *Advances in Water Science*, 24,
718 901-908, 2013.
719 Coccia, G., and Todini, E.: Recent developments in predictive uncertainty assessment based on the
720 model conditional processor approach, *Hydrol. Earth Syst. Sci.*, 15, 3253-3274,
721 <https://doi.org/10.5194/hess-15-3253-2011>, 2011.
722 Collier, C. G.: Flash flood forecasting: What are the limits of predictability? *Q. J. R. Meteorol. Soc.*,
723 133, 3-23, <https://doi.org/10.1002/qj.29>, 2007.
724 Confalonieri, R., Bellocchi, G., Bregaglio, S., Donatelli, M., and Acutis, M.: Comparison of sensitivity
725 analysis techniques: A case study with the rice model WARM, *Ecol. Model.*, 221, 1897-1906,
726 <https://doi.org/10.1016/j.ecolmodel.2010.04.021>, 2010.
727 Cools, J., Innocenti, D., and O'Brien, S.: Lessons from flood early warning systems, *Environ. Sci.*
728 *Policy*, 58, 117-122, <https://doi.org/10.1016/j.envsci.2016.01.006>, 2016.
729 Du, E., Cai, X., Sun, Z., and Minsker, B.: Exploring the Role of Social Media and Individual Behaviors
730 in Flood Evacuation Processes: An Agent-Based Modeling Approach, *Water Resour. Res.*, 53,
731 9164-9180, <https://doi.org/10.1002/2017WR021192>, 2017.
732 Duc Anh, D., Kim, D., Kim, S., and Park, J.: Determination of flood-inducing rainfall and runoff for
733 highly urbanized area based on high-resolution radar-gauge composite rainfall data and flooded area
734 GIS data, *J. Hydrol.*, 584, 124704, <https://doi.org/10.1016/j.jhydrol.2020.124704>, 2020.
735 Han, S. S., and Coulibaly, P.: Bayesian flood forecasting methods: A review, *J. Hydrol.*, 551, 340-351,
736 <https://doi.org/10.1016/j.jhydrol.2017.06.004>, 2017.
737 Hicks, F. E., and Peacock, T.: Suitability of HEC-RAS for Flood Forecasting, *Canadian Water*
738 *Resources Journal / Revue canadienne des ressources hydriques*, 30, 159-174,
739 <https://doi.org/10.4296/cwrj3002159>, 2005.
740 Janssen, M. A., and Ostrom, E.: Empirically based, agent-based models, *Ecol. Soc.*, 11, 37, 2006.
741 Jauernic, S. T., and Van den Broeke, M. S.: Tornado Warning Response and Perceptions among
742 Undergraduates in Nebraska, *Weather Clim. Soc.*, 9, 125-139,
743 <https://doi.org/10.1175/WCAS-D-16-0031.1>, 2017.
744 Ke, Q., Tian, X., Bricker, J., Tian, Z., Guan, G., Cai, H., Huang, X., Yang, H., and Liu, J.: Urban
745 pluvial flooding prediction by machine learning approaches-a case study of Shenzhen city, China, *Adv.*
746 *Water Resour.*, 145, 103719, <https://doi.org/10.1016/j.advwatres.2020.103719>, 2020.
747 Krzysztofowicz, R.: The case for probabilistic forecasting in hydrology, *J. Hydrol.*, 249, 2-9,
748 [https://doi.org/10.1016/S0022-1694\(01\)00420-6](https://doi.org/10.1016/S0022-1694(01)00420-6), 2001.
749 LeClerc, J., and Joslyn, S.: The Cry Wolf Effect and Weather-Related Decision Making, *Risk Anal.*, 35,
750 385-395, <https://doi.org/10.1111/risa.12336>, 2015.
751 Lei, X., Wang, H., Liao, W., Yang, M., and Gui, Z.: Advances in hydro-meteorological forecast under
752 changing environment, *J. Hydraul. Eng.-ASCE*, 49, 9-18, 2018.
753 Lim, J. R., Liu, B. F., and Egnoto, M.: Cry Wolf Effect? Evaluating the Impact of False Alarms on
754 Public Responses to Tornado Alerts in the Southeastern United States, *Weather Clim. Soc.*, 11,
755 549-563, <https://doi.org/10.1175/WCAS-D-18-0080.1>, 2019.
756 Lo, S. M., Fang, Z., Lin, P., and Zhi, G. S.: An evacuation model: the SGEM package, *Fire Saf. J.*, 39,
757 169-190, <https://doi.org/10.1016/j.firesaf.2003.10.003>, 2004.
758 Maidment, D. R.: CONCEPTUAL FRAMEWORK FOR THE NATIONAL FLOOD
759 INTEROPERABILITY EXPERIMENT, *J. Am. Water Resour. Assoc.*, 53, 245-257,
760 <https://doi.org/10.1111/1752-1688.12474>, 2017.
761 Mileti, D. S.: Factors Related to Flood Warning Response, in: *Research Workshop on the*
762 *Hydrometeorology, Impacts, and Management of Extreme Floods, Perugia (Italy)*, 1995.



- 763 Oakley, J. E., and O'Hagan, A.: Probabilistic sensitivity analysis of complex models: a Bayesian
764 approach, *J. R. Stat. Soc. Ser. B-Stat. Methodol.*, 66, 751-769,
765 <https://doi.org/10.1111/j.1467-9868.2004.05304.x>, 2004.
- 766 O'Hagan, A.: Bayesian analysis of computer code outputs: A tutorial, *Reliab. Eng. Syst. Saf.*, 91,
767 1290-1300, <https://doi.org/10.1016/j.res.2005.11.025>, 2006.
- 768 Oleyiblo, J. O., and Li, Z.: Application of HEC-HMS for flood forecasting in Misai and Wan'an
769 catchments in China, *Water Sci. Eng.*, 3, 14-22,
770 <https://doi.org/https://doi.org/10.3882/j.issn.1674-2370.2010.01.002>, 2010.
- 771 Parker, D. J., Priest, S. J., and Tapsell, S. M.: Understanding and enhancing the public's behavioural
772 response to flood warning information, *Meteorol. Appl.*, 16, 103-114, <https://doi.org/10.1002/met.119>,
773 2009.
- 774 Potter, S., Harrison, S., and Kreft, P.: The Benefits and Challenges of Implementing Impact-Based
775 Severe Weather Warning Systems: Perspectives of Weather, Flood, and Emergency Management
776 Personnel, *Weather Clim. Soc.*, 13, 303-314, <https://doi.org/10.1175/WCAS-D-20-0110.1>, 2021.
- 777 Ramos Filho, G. M., Rabelo Coelho, V. H., Freitas, E. D. S., Xuan, Y., and Neves Almeida, C. S.: An
778 improved rainfall-threshold approach for robust prediction and warning of flood and flash flood
779 hazards, *Nat. Hazards*, 105, 2409-2429, <https://doi.org/10.1007/s11069-020-04405-x>, 2021.
- 780 Ripberger, J. T., Silva, C. L., Jenkins-Smith, H. C., Carlson, D. E., James, M., and Herron, K. G.: False
781 Alarms and Missed Events: The Impact and Origins of Perceived Inaccuracy in Tornado Warning
782 Systems, *Risk Anal.*, 35, 44-56, <https://doi.org/10.1111/risa.12262>, 2015.
- 783 Roulston, M. S., and Smith, L. A.: The Boy who Cried Wolf revisited: The impact of false alarm
784 intolerance on cost-loss scenarios, *Weather Forecast.*, 19, 391-397,
785 [https://doi.org/10.1175/1520-0434\(2004\)019<0391:TBWCWR>2.0.CO;2](https://doi.org/10.1175/1520-0434(2004)019<0391:TBWCWR>2.0.CO;2), 2004.
- 786 Sawada, Y., Kanai, R., and Kotani, H.: Impact of cry wolf effects on social preparedness and the
787 efficiency of flood early warning systems, *Hydrol. Earth Syst. Sci.*, 26, 4265-4278,
788 <https://doi.org/10.5194/hess-26-4265-2022>, 2022.
- 789 Shanghai Meteorological Bureau: Rainstorm warning signal, 2019
- 790 Simmons, K. M., and Sutter, D.: False Alarms, Tornado Warnings, and Tornado Casualties, *Weather
791 Clim. Soc.*, 1, 38-53, <https://doi.org/10.1175/2009WCAS1005.1>, 2009.
- 792 Sivapalan, M., and Bloeschl, G.: Time scale interactions and the coevolution of humans and water,
793 *Water Resour. Res.*, 51, 6988-7022, <https://doi.org/10.1002/2015WR017896>, 2015.
- 794 Slater, L., Villarini, G., Archfield, S., Faulkner, D., Lamb, R., Khouakhi, A., and Yin, J.: Global
795 Changes in 20-Year, 50-Year, and 100-Year River Floods, *Geophys. Res. Lett.*, 48, e2020GL091824,
796 <https://doi.org/10.1029/2020GL091824>, 2021.
- 797 Tekeli, A. E., and Fouli, H.: Reducing False Flood Warnings of TRMM Rain Rates Thresholds over
798 Riyadh City, Saudi Arabia by Utilizing AMSR-E Soil Moisture Information, *Water Resour. Manag.*, 31,
799 1243-1256, <https://doi.org/10.1007/s11269-017-1573-1>, 2017.
- 800 Todini, E.: Flood Forecasting and Decision Making in the new Millennium. Where are We? *Water
801 Resour. Manag.*, 31, 3111-3129, <https://doi.org/10.1007/s11269-017-1693-7>, 2017.
- 802 Wang, L., Nie, R. H., Slater, L. J., Xu, Z. H., Guan, D. W., and Yang, Y. F.: Education can improve
803 response to flash floods, *Science*, 377, 1391-1392, <https://doi.org/10.1126/science.ade6616>, 2022.
- 804 Wang, Z. Q., Huang, J., Wang, H. M., Kang, J. L., and Cao, W. W.: Analysis of Flood Evacuation
805 Process in Vulnerable Community with Mutual Aid Mechanism: An Agent-Based Simulation
806 Framework, *INTERNATIONAL JOURNAL OF ENVIRONMENTAL RESEARCH AND PUBLIC
807 HEALTH*, 17, 560, <https://doi.org/10.3390/ijerph17020560>, 2020.
- 808 Wei, L.: Extreme heavy rainfall in Liulin Town, Suixian County, Hubei Province has resulted in 21
809 deaths and 4 loss of contact, 2021
- 810 Wu, S., Lei, Y., Yang, S., Cui, P., and Jin, W.: An Agent-Based Approach to Integrate Human
811 Dynamics Into Disaster Risk Management, *Front. Earth Sci.*, 9, 818913,
812 <https://doi.org/10.3389/feart.2021.818913>, 2022.
- 813 Yang, L. E., Scheffran, J., Suessner, D., Dawson, R., and Chen, Y. D.: Assessment of Flood Losses with
814 Household Responses: Agent-Based Simulation in an Urban Catchment Area, *Environ. Model. Assess.*,
815 23, 369-388, <https://doi.org/10.1007/s10666-018-9597-3>, 2018.
- 816 Yin, J., Gao, Y., Chen, R., Yu, D., Wilby, R., Wright, N., Ge, Y., Bricker, J., Gong, H., and Guan, M.:
817 Flash floods: why are more of them devastating the world's driest regions? *Nature*, 615, 212-215,
818 <https://doi.org/10.1038/d41586-023-00626-9>, 2023.
- 819 Young, A., Bhattacharya, B., and Zevenbergen, C.: A rainfall threshold-based approach to early
820 warnings in urban data-scarce regions: A case study of pluvial flooding in Alexandria, Egypt, *J. Flood
821 Risk Manag.*, 14, e12702, <https://doi.org/10.1111/jfr3.12702>, 2021.
- 822 Younis, J., Anquetin, S., and Thielen, J.: The benefit of high-resolution operational weather forecasts



823 for flash flood warning, *Hydrol. Earth Syst. Sci.*, 12, 1039-1051,
824 <https://doi.org/10.5194/hess-12-1039-2008>, 2008.
825 Zhai, X., Guo, L., Liu, R., and Zhang, Y.: Rainfall threshold determination for flash flood warning in
826 mountainous catchments with consideration of antecedent soil moisture and rainfall pattern, *Nat.*
827 *Hazards*, 94, 605-625, <https://doi.org/10.1007/s11069-018-3404-y>, 2018.
828 Zhang, R., Liu, D., Du, E., Xiong, L., Chen, J., and Chen, H.: An agent-based model to simulate human
829 responses to flash flood warnings for improving evacuation performance, *J. Hydrol.*, 628, 130452,
830 <https://doi.org/https://doi.org/10.1016/j.jhydrol.2023.130452>, 2024.
831 Zhuo, L., and Han, D. W.: Agent-based modelling and flood risk management: A compendious
832 literature review, *J. Hydrol.*, 591, 125600, <https://doi.org/10.1016/j.jhydrol.2020.125600>, 2020.
833